Journal of Biomolecular NMR, 10 (1997) 187–192
KLUWER/ESCOM
© 1997 *Kluwer Academic Publishers. Printed in The Netherlands.*

J-Bio NMR 476

A new method to determine DNA sugar conformation from the joint use of 2D and 3D NMR data

Mounia Chaoui, Olivier Mauffret, Anne Lefebvre, Elie Lescot, Georges Tevanian and Serge Fermandjian*

Département de Biologie et Pharmacologie Structurales, URA 147 CNRS, Institut Gustave Roussy, P.R. 2, 39 rue Camille Desmoulins, F-94805 Villejuif Cedex, France

Received 28 April 1997
Accepted 23 July 1997

Keywords: B-DNA; 3D NOE-NOE; Sugar conformation

Summary

The use of sugar restraints has been proven essential for assessing DNA structures through molecular modeling studies. We present a new method combining 2D (COSY and NOESY) and 3D (NOESY-NOESY) experiments, where constraints on either the phase angles or the difference between phase angles of two residues are obtained from comparison of 2D NOE H1'-H4' intensities and 3D NOE intensities containing the H1'-H4' transfer. All experiments lead to restraints that match, proving the validity of the method.

A large number of studies have shown that sugar conformations play a fundamental role in fashioning the DNA double helix structure (Mauffret et al., 1992; Poncin et al., 1992; Lefebvre et al., 1995). Thus, accurate NMR constraints on sugar phases are needed in a DNA modeling strategy. Pseudorotational angles of sugars are generally obtained by using a combination of various methods based upon (i) simulation of COSY cross peaks (Widmer and Wüthrich, 1987); (ii) measurements of COSY coupling sums (Van Wijk et al., 1992); (iii) determination of COSY coupling constants (Hosur et al., 1986; Kim et al., 1992); and (iv) determination of NOE distances (Wüthrich, 1986). Yet, the above measurements are not always feasible, as large DNA molecules often lead either to too broad NMR signals, precluding access to sugar conformation via (i) and (ii), or to signal overlappings in 2D spectra.

We present a procedure combining 2D and 3D experiments and providing the H1'-H4' intranucleotide distance, which is strongly related to the sugar conformation. Studies were carried out with a 15-mer pseudopalindromic B-DNA, d(GAGATGACTCATCTC/GAGATGAGTCATCTC) (Fig. 1), which is hereafter denoted TRE-15. In its center, TRE-15 encompasses the heptanucleotide TRE (TPA Responsive Element) specifically recognized by bZIP proteins of the AP-1 family during the transcription process (reviewed by Karin et al., 1997).

So far (see below), 3D ^{1}H NOE-NOEs have been used according to two different procedures for the determination of macromolecule structures. Distances have been derived from 3D intensities using the approximation $I_{ijk} \propto r_{ij}^{-6} r_{jk}^{-6}$, where I_{ijk} is the 3D NOE intensity and r values are distance constraints involved in the 3D connectivity (Holak et al., 1991). In a more accurate approach, 3D cross-peak NOE intensities have been used directly in structure calculations (Bonvin et al., 1991; Habazettl et al., 1992; Bernstein et al., 1993). The present method proceeds through the comparison of 3D NOE intensities. Since

$$I_{3D}[\text{H4'-H1'-X}] \propto I_{2D}[\text{H1'-H4'}]_{intra} * I_{2D}[\text{H1'-X}] \qquad (1)$$

where X stands for any proton detected in the acquisition dimension (Boelens et al., 1989; Griesinger et al., 1989; Habazettl et al., 1992; Donne et al., 1995), when the I_{2D}[H1'-X] values are similar, comparing I_{3D}[H4'-H1'-X] of one peak to that of another peak is equivalent to comparing the 2D NOE intensities $I_{2D}[\text{H1'-H4'}]_{intra}$.

*To whom correspondence should be addressed.

5' G_1 A_2 G_3 A_4 T_5 G_6 A_7 C_8 T_{10} C_{11} A_{12} T_{13} C_{14} T_{15} C_{16} 3' (TRE[C])

3' C_{32} T_{31} C_{30} T_{29} A_{28} C_{27} T_{26} G_{25} A_{23} G_{22} T_{21} A_{20} G_{19} A_{18} G_{17} 5' (TRE[G])

Fig. 1. Sequence of the TRE-15 DNA fragment analyzed in this work. For use in future comparisons, residues are numbered to adopt the numbering of residues in CRE-16, which is related to TRE-15 through an additional base pair (G_9 C_{24}). The consensus functional sequence TRE is boxed. The duplex was dissolved at 3 mM concentration in a phosphate buffer containing 1 mM EDTA at pH 7, ionic strength I = 0.1. NMR experiments were performed in D_2O at 30 °C on a Bruker AMX 500 spectrometer. Spectra were then processed on an X32 Bruker station or a Silicon Graphics INDIGO R4000 workstation with the FELIX software (v. 2.35).

As visualized in Fig. 2, where H1'-H4' intraresidue 2D NOE cross-peak intensities are found in the same increasing order at mixing times from 50 to 300 ms, H1'-H4' intranucleotide distances are distorted only to a small extent by the spin diffusion effect (Chuprina et al., 1993). This phenomenon is likely due to the fact that in B-DNA, the H1' and H4' sugar protons are in close spatial proximity (2.6–3.6 Å) and their distances to neighboring protons either do not vary significantly (in the case of H1'-H2", H1'-H2' and H3'-H4') or are very large (in the case of H2"-H4'). Thus, comparing the $I_{2D}[H1'\text{-}H4']_{intra}$ values measured at 300 ms mixing time is equivalent to comparing the H4'-H1' intraresidue distances and, hence, the

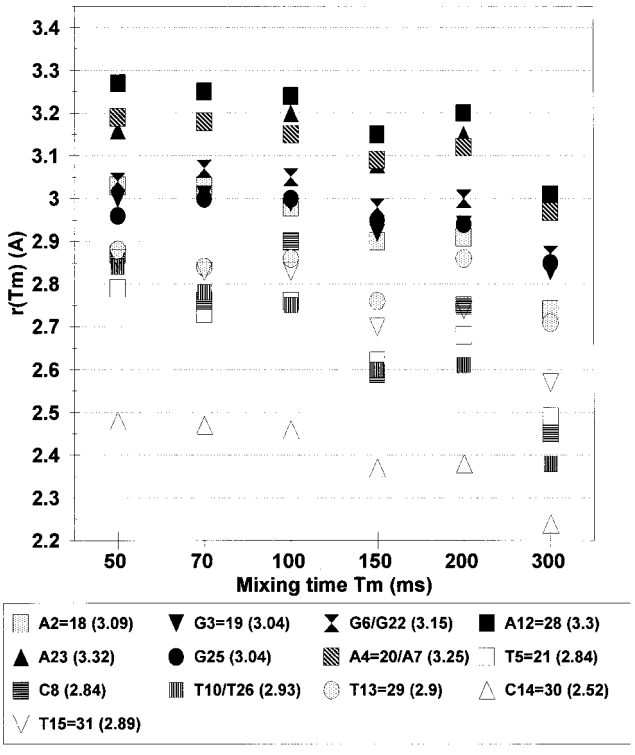

Fig. 2. $r[H1'\text{-}H4'](T_m) = r_{ref}*[V_{ref}(T_m)/V(T_m)]^{1/6}$ as a function of the mixing time T_m. V is the NOE volume; V_{ref} is the NOE volume of the reference cross peak, which is the non-terminal H5-H6 cytosine correlation; r_{ref} is the reference distance, which is the non-terminal H5-H6 cytosine distance taken equal to 2.5 Å. / means overlapped peaks and = means identical residues. Distances indicated in parentheses are in Å and were estimated using the extrapolation method (Baleja et al., 1990a,b; Mauffret et al., 1992) as a first order correction for spin diffusion effects: $d[H1'\text{-}H4'] = \lim_{T_m \to 0} r[H1'\text{-}H4'](T_m)$.

TABLE 1
CONSTRAINTS APPLIED TO PSEUDOROTATIONAL ANGLES

Phase (°) (min < Pn <max)	Difference of phases (°)
140 < P2=P18 < 180	P12–P2 > 15
115 < P3=P19 < 175	P12–P3 > 15
115 < P5 < 145	P23–P2 > 15
115 < P8 < 145	P23–P3 > 15
110 < P10 < 155	
110 < P11 < 155	P3–P5 > 10
135 < P12 < 200	P4–P5 > 10
120 < P13=P29 < 145	P12–P4 > 10
90 < P14=P30 < 110	P6–P22 > 10
120 < P15=P31 < 145	
115 < P21 < 145	−5 < P23–P7 < 5
135 < P23 < 200	
115 < P25 < 145	P4 = P20
110 < P26 < 160	
110 < P27 < 155	
135 < P28 < 200	

Underlined restraints were determined by 2D experiments (NOESY and COSY). A DQF (double quantum filtered)-COSY (Piantini et al., 1982; Rance et al., 1983) was recorded. Data were collected with 4096 points in the acquisition dimension t_2 and 700 points in t_1, with a spectral width of 5050 Hz in each dimension; the relaxation delay was 1.5 s. Data were apodized using sine-bells, 60° shifted in the t_2 dimension and 30° phase shifted in the t_1 dimension and zero-filled after Fourier transformation to obtain a 4096 × 2048 real matrix. Quantitative 2D NOE experiments were recorded at six different mixing times with a spectral width of 4504 Hz. A recycle delay of 2 s was used, as this is enough to provide relaxation of all protons, except adenine H2 protons (Lefebvre et al., 1995). A total of 800 experiments (t_1) were performed with 1024 (t_2) complex points acquired for each FID. For each t_1, 32 scans were collected. t_1 and t_2 data were apodized with a sine-squared 90° phase-shifted function and a sine-squared 60° phase-shifted function, respectively. Two dimensions were zero-filled to 2048 points. Baseline correction was performed with a baseline convolution method (Dietrich et al., 1991). The input precision for distances H1'-H4' is ±0.4 Å for distances greater than 3.0 Å and ±0.2 Å for distances between 2.5 and 3.0 Å (Lefebvre et al., 1995). This takes into account the difference of intensities between cross peaks up and down the spectrum diagonal, spin diffusion effects and extrapolation back to zero mixing time. Input precision for the phases and phase differences are determined as follows. In Wüthrich (1986), H1'-H4' distances as a function of P display an almost straight line for 120° < P < 200° with 40° representing 0.5 Å. For H1'-H4' distances greater than 3.0 Å or lower than 3.0 Å, the input precision for distances is 0.8 Å and 0.4 Å, respectively. Thus, for distances greater than 3.0 Å and for distances lower than 3.0 Å, precision inputs for P result in 60° and 30°, respectively. The average difference between H1'-H4' cross peaks along the diagonal is found around 0.05 Å, corresponding to a P difference of 5°, which allowed 5° increments for P difference constraints.

pseudorotational angles (Wüthrich, 1986). Since the accuracy of measurements is higher at longer mixing times, we use hereafter 3D intensities collected at 300 ms. This provides a set of constraints based on differences between the phases of two residues. Such constraints are less stringent compared to constraints on a single angle and lead to a lower energy cost in molecular modeling.

As TRE-15 is not palindromic (Fig. 1), its two strands do not display an identical NOE correlation pathway across the consensus sequence (data not shown). The differences decrease progressively from the center of the molecule to each extremity and can no longer be detected on the external base pairs: $A_{2=18}$, $G_{3=19}$, $A_{4=20}$, $T_{5=21}$, $A_{12=28}$, $T_{13=29}$, $C_{14=30}$ and $T_{15=31}$.

2D experiments (NOESY and COSY) provide a first set of pseudorotational constraints (Table 1) via (iii) and (iv) listed above. A model implying a fast equilibrium between several sugar conformations is not considered, since our experimental values can be fit through a single South-state conformation (see for instance Gochin and James, 1990; Gochin et al., 1990).

The COSY spectra yield: ^{3}J(H1'H2') > ^{3}J(H1'H2"), and thus $90° < P < 200°$ (P designates the phase angle) for every sugar. For such a P range, the P values determined from H1'-H4' distances (Fig. 2; Wüthrich, 1986) and ^{3}J(H3'H4') and ^{3}J(H3'H2') coupling constants measured from COSY cross-peak intensities (Hosur et al., 1986; Kim et al., 1992) are less than 145° for pyrimidines C_8, $T_{13} = T_{29}$ and $T_{15} = T_{31}$. We note that the purine G_{25} is also characterized by strong ^{3}J(H3'H4') and ^{3}J(H3'H2') coupling constants, in favor of a P value less than 145°, while $A_{2=18}$ displays a very weak ^{3}J(H3'H4') coupling constant, in favor of a P value greater than 140°. For $C_{14=30}$, the presence of a H2"-H3' cross peak in the COSY spectrum and a small H1'-H4' distance value (Fig. 2) confer to this residue an East sugar conformation (O1'-endo).

Both molecular mechanics studies (Poncin et al., 1992) and experimental results (Mauffret et al., 1992; Chuprina et al., 1993; Lefebvre et al., 1995) have confirmed that pyrimidines prefer P values lying between 90° and 160°, and purines prefer P values between 140° and 200°. For purines, two cases are possible: either $140° < P < 170°$, generally related to a high amplitude value (>40°), or $170° < P < 200°$, more compatible with a low amplitude value (<38°).

The purine P values are determined more accurately by comparing r values of the H1'-H4' NOEs at all mixing times, and the corresponding H1'-H4' distances given by the extrapolation method, without taking into account the input precision. NOE intensity differences reflect distance differences, and thus phase differences. At each mixing time, the above r values found for A_{23} and $A_{12=28}$ are larger by 0.15 Å or more than the r values for $A_{2=18}$ and $G_{3=19}$ (Fig. 2). At the same time, distances provided by the extrapolation method are about 3.3 Å for A_{23} and $A_{12=28}$, and 3/3.1 Å for $A_{2=18}$ and $G_{3=19}$. Differences observed between the above two sets of residues yield a phase angle difference of roughly 15° (Table 1). For $T_{5=21}$, the extrapolation method provides an H1'-H4' intranucleotide distance of about 2.8 Å, and at each mixing time the distance value is 0.2 Å shorter compared to the distance found for $G_{3=19}$ (Fig. 2), corresponding to a difference $P3 - P5 > 10°$ (Table 1).

In summary, residues can be gathered in three groups: pyrimidines ($T_{5=21}$, $T_{13=29}$, $T_{15=31}$, C_8), characterized by the smallest H1'-H4' distances and phase angles; purines ($A_{2=18}$, $G_{3=19}$) with medium H1'-H4' distances and phase angles; and purines ($A_{12=28}$ and A_{23}) showing the largest H1'-H4' distances and phase angles.

2D NOE signal overlap prevents the conformational analysis of many sugars (Fig. 1). This overlap concerns, for instance, the H1'-H4' NOE cross peaks of $A_{4=20}$ and A_7 (Table 2). The global peak intensity is measured at each mixing time, divided by three, and the resulting value is compared to non-overlapped peak intensities. The thus estimated average intensity is found to be comparable to cross-peak intensities displayed by adenines A_{23}

TABLE 2
SOME PROTON CHEMICAL SHIFTS (H68, CH3, H1' AND H4') (ppm) OF TRE-15 AT 30 °C

	CH3 (T)	Bases H68	Sugars	
			H1'	H4'
G1		7.74	5.46	4.06
A2		8.07	5.88	4.3
G3		7.58	5.53	4.3
A4		7.99	6.11	4.35
T5	1.2	6.91	5.55	4
G6		7.69	5.4	4.22
A7		8.03	6.09	4.35
C8		7.1	5.62	4.05
T10	1.37	7.24	5.88	3.96
C11		7.39	5.43	4.01
A12		8.2	6.14	4.31
T13	1.31	7.08	5.76	4.1
C14		7.47	5.87	4.07
T15	1.6	7.41	6.02	4.09
C16		7.58	6.18	3.93
G17		7.74	5.46	4.06
A18		8.07	5.88	4.3
G19		7.58	5.53	4.3
A20		7.99	6.11	4.35
T21	1.2	6.9	5.55	4
G22		7.69	5.39	4.2
A23		7.95	5.96	4.33
G25		7.37	5.69	4.24
T26	1.06	7.05	5.86	4
C27		7.39	5.46	4.06
A28		8.2	6.14	4.31
T29	1.31	7.08	5.76	4.1
C30		7.47	5.87	4.07
T31	1.6	7.41	6.02	4.09
C32		7.58	6.18	3.93

TABLE 3
USED 2D AND 3D NOE INTENSITIES AT 300 ms

2D cross peaks		Percentage of similarity $2*[I_A-I_B]/[I_A+I_B]$	Peaks [ω1-ω2-ω3] to be compared	Intensities to be compared
Intensities I_A	Intensities I_B			
H1'(G_{25})-CH3(T_{26}) 159	H1'(C_8)-CH3(T_{10}) 141		[H4'(C_8)-H1'(C_8)-CH3(T10)]	0.276
		12	[H4'(G_{25})-H1'(G_{25})-CH3(T_{26})]	absent (<0.1)
H1'(C_8)-H6(T_{10}) 103	H1'(G_{25})-H6(T_{26}) 114		[H4'(C_8)-H1'(C_8)-H6(T_{10})]	0.87
		10	[H4'(G_{25})-H1'(G_{25})-H8(T_{26})]	<0.1
H1'($T_{5=21}$)-H6($T_{5=21}$) 283	H1'($G_{3=19}$)-H8($G_{3=19}$) 288		[H4'($T_{5=21}$)-H1'($T_{5=21}$)-H6($T_{5=21}$)]	1.34
		2	[H4'($G_{3=19}$)-H1'($G_{3=19}$)-H8($G_{3=19}$)]	0.427
H1'($A_{2=18}$)-H8($A_{2=18}$) 364	H1'($T_{5=21}$)-H6($T_{5=21}$) 283		[H4'($A_{2=18}$)-H1'($A_{2=18}$)-H8($A_{2=18}$)]	0.48
			[H4'($T_{5=21}$)-H1'($T_{5=21}$)-H6($T_{5=21}$)]	1.34
H1'($A_{12=28}$)-H6($T_{13=29}$) 304	H1'($A_{4=20}$)-H6($T_{5=21}$) 304		[H4'($A_{12=28}$)-H1'($A_{12=28}$)-H6($T_{13=29}$)]	<0.5
		0	[H4'($A_{4=20}$)-H1'($A_{4=20}$)-H6($T_{5=21}$)]	1.41
H1'($T_{5=21}$)-H8($G_{6/22}$) 215	H1'($A_{4=20}$)-H6($T_{5=21}$) 304		[H4'($A_{4=20}$)-H1'($A_{4=20}$)-H6($T_{5=21}$)]	1.41
			[H4'($T_{5=21}$)-H1'($T_{5=21}$)-H8($G_{6/22}$)]	3.26
H1'(A_7)-H6(C_8) 168	H1'(A_{23})-H8(G_{25}) 169		[H4'(A_7)-H1'(A_7)-H6(C_8)]	<0.5
		1	[H4'(A_{23})-H1'(A_{23})-H8(G_{25})]	0.5
H1'(C_{11})-H8(A_{12}) 119	H1'(C_{27})-H8(A_{28}) 128			
		7		
H1'($C_{11/27}$)-H8($A_{12=28}$) 247	H1'($T_{5=21}$)-H8($G_{6/22}$) 215		[H4'($C_{11/27}$)-H1'($C_{11/27}$)-H8($A_{12=28}$)]	2.00
		14	[H4'($T_{5=21}$)-H1'($T_{5=21}$)-H8($G_{6/22}$)]	3.26
H1'(G_6)-H8(A_7) 199	H1'(G_{22})-H8(A_{23}) 214		[H4'(G_6)-H1'(G_6)-H8(A_7)]	absent (<0.1)
		7	[H4'(G_{22})-H1'(G_{22})-H8(A_{23})]	1.42
H1'(T_{10})-H6(T_{10}) 146	H1'(A_{23})-H8(A_{23}) 160		[H4'(T_{10})-H1'(T_{10})-H6(T_{10})]	1.32
		9	[H4'(A_{23})-H1'(A_{23})-H8(A_{23})]	absent (<0.1)

A slash means overlapped cross peaks.

and $A_{12=28}$, which in fact correspond to the smallest intensities (Fig. 2). We thus conclude that the P values of $A_{4=20}$ and A_7 are similar to those of A_{23} and $A_{12=28}$. The intensity of the overlapped cross peaks of T_{10} and T_{26}, once divided by two, is similar to intensities of non-overlapped pyrimidine cross peaks at each mixing time (Fig. 2). Short H1'-H4' r values are thus derived for T_{10} and T_{26} and are compatible with phase angles less than 155°. For each mixing time, the intensity of overlapped H1'-H4' NOE cross peaks of G_6 and G_{22} (Table 2), divided by two, provides an intermediate value between the intensities of the A_{23} and G_3 cross peaks. In this case, there are three possibilities: the P values of both G_6 and G_{22} can be intermediate between those of A_{23} and G_3; the P value of G_6 can be comparable to the one of G_3 and that of G_{22} comparable to the one of A_{23}; and, conversely, the P value of G_6 can be comparable to the one of A_{23} and that of G_{22} comparable to the one of G_3. As for C_{11} and C_{27}, no information can be obtained from 2D experiments (Table 2).

A 3D NOE-NOE experiment has been conducted to obtain more reliable information on P values. Three magnetization transfers containing the intranucleotide H1'→H4' transfer, i→j→k [(ω1)→(ω2)→(ω3)] (k is the proton detected in the acquisition dimension) are considered for a nucleotide denoted n, with n+1 being the following nucleotide on the 3' side: (1) H4'(n)→H1'(n)→H68(n); (2) H4'(n)→H1'(n)→H68(n+1) and (3) H4'(n)→H1'(n)→CH3(n+1). Among these chemical shifts, CH3 and H68 present the opportunity to be well separated (Table 2).

By starting with residues whose 2D H1'-H4' cross peaks are not overlapped, the validity of our method was checked. We selected residues C_8 and G_{25} and used the above mentioned correlation way (3). The 2D NOE H1'(n)-CH3(n+1) cross peaks of these two residues are not overlapped (Table 2) and, at 300 ms mixing time, differ by only 12% (Table 3). The 3D cross-peak intensity at 300 ms mixing time is proportional to the intensity product of the two successive 2D NOE transfers at 300 ms (H4'(n)→H1'(n) and then H1'(n)→CH3(n+1)). Since I_{2D}[CH3(n+1)-H1'(n)] of C_8 and G_{25} are similar, comparing I_{3D}[H4'(n)-H1'(n)-CH3(n+1)] of C_8 and G_{25} at 300 ms is equivalent to comparing their I_{2D}[H1'(n)-H4'(n)] cross peaks at 300 ms. As I_{3D}[H4'(C_8)-H1'(C_8)-CH3(T_{10})] is greater than I_{3D}[H4'(G_{25})-H1'(G_{25})-CH3(T_{26})] (Table 3 and Fig. 3), we deduce that I_{2D}[H4'-H1'](C_8) is greater than I_{2D}[H4'-H1'](G_{25}) at 300 ms. This confirms the above 2D NOE results, where r[H4'-H1'](G_{25})(300 ms) (2.85 Å) is found to be greater than r[H4'-H1'](C_8)(300 ms) (2.45 Å) ($r = r_{ref}*(V_{ref}/V)^{1/6}$) (Fig. 2). The same reasoning applied to [H4'(C_8)-H1'(C_8)-H6(T_{10})] and [H4'(G_{25})-H1'(G_{25})-H6(T_{26})] (magnetization transfer (2)) provides the same result (Table 3).

The validity of our method is then checked with $T_{5=21}$ and $G_{3=19}$ (Table 2). Selection of well-separated H6 ($T_{5=21}$) and H8 ($G_{3=19}$) planes permits the comparison of I_{3D}[H4'($G_{3=19}$)-H1'($G_{3=19}$)-H8($G_{3=19}$)] and I_{3D}[H4'($T_{5=21}$)-

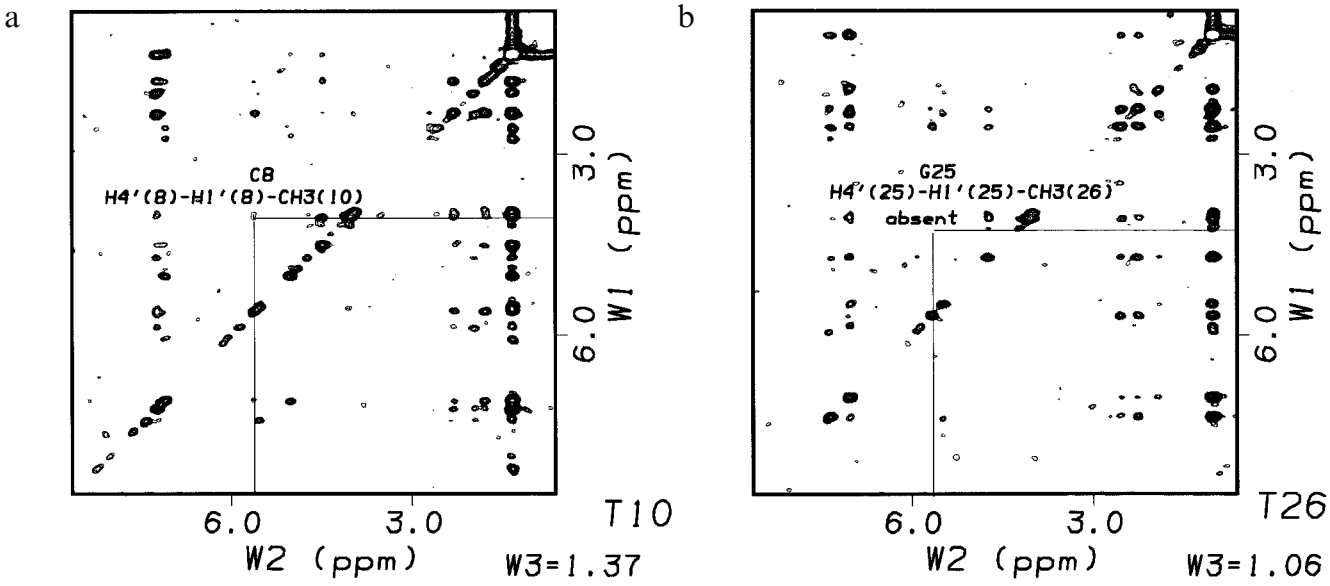

Fig. 3. ω3 (acquisition dimension) sections of the 3D NOE-NOE spectrum. Sections are labelled with the residue number and interesting resonances are labelled with the residue number and the correlation pathway. The 3D experiment was conducted according to Boelens et al. (1989) with a spectral width of 4032 Hz in each of the three dimensions. It was recorded at 300 ms NOE mixing times in both steps of the magnetization transfer. Eight scans were collected and the relaxation time was 2 s. The data consisted of $1024 \times 128 \times 200$ real points in the t_3, t_2 and t_1 dimensions, respectively. t_2 and t_1 data points were processed with a sine-squared 90° phase-shifted function and the t_3 data points with a sine-squared 60° phase-shifted function. The acquisition dimension was zero-filled to 2048 points and the other two dimensions to 256 points.

H1'($T_{5=21}$)-H6($T_{5=21}$)] (magnetization transfer (1)). Table 3 and the preceding reasoning indicate that I_{2D}[H4'($G_{3=19}$)-H1'($G_{3=19}$)] is less than I_{2D}[H4'($T_{5=21}$)-H1'($T_{5=21}$)]. As H1'-H4' intranucleotide distances are only weakly distorted by spin diffusion (Chuprina et al., 1993; Fig. 2), $d_{H4'H1'}G_{3=19}$ is greater than $d_{H4'H1'}T_{5=21}$ and $P_{T5=21}$ is less than $P_{G3=19}$, confirming the 2D results presented in Table 1.

H1'-H4' intranucleotide cross peaks of neither $A_{2=18}$ nor $T_{5=21}$ are overlapped (Table 2). Comparison of I_{3D}[H4'($A_{2=18}$)-H1'($A_{2=18}$)-H8($A_{2=18}$)] with I_{3D}[H4'($T_{5=21}$)-H1'($T_{5=21}$)-H6($T_{5=21}$)] (magnetization transfer (1)) shows that the first intensity is less than the second one, while I_{2D}[H1'($A_{2=18}$)-H8($A_{2=18}$)] is found to be stronger than I_{2D}[H1'($T_{5=21}$)-H6($T_{5=21}$)] at 300 ms. As the 3D intensity is proportional to the product of the two 2D intensities, I_{2D}[H4'($A_{2=18}$)-H1'($A_{2=18}$)] at 300 ms is weaker than I_{2D}[H4'($T_{5=21}$)-H1'($T_{5=21}$)] and the same arguments as in the preceding paragraph show that P_{T5} is less than P_{A2}, agreeing with the 2D results (Table 1).

Adenines $A_{4=20}$, A_7, $A_{12=28}$ and A_{23} and thymine $T_{5=21}$ provide good examples of the application of this new method. The H1'-H4' intranucleotide NOE cross peak of $A_{4=20}$ is found to overlap with that of A_7 in 2D spectra (Table 2). Concerning $A_{4=20}$ and $A_{12=28}$, distinct chemical shifts for H6($T_{13=29}$) and H6($T_{5=21}$) permit the selection of H68(n+1) (ω3) planes (Table 2), i.e. [H4'($A_{12=28}$)-H1'($A_{12=28}$)-H6($T_{13=29}$)] and [H4'($A_{4=20}$)-H1'($A_{4=20}$)-H6($T_{5=21}$)] magnetization transfers. From Table 3 and the preceding reasonings, we conclude that $P_{A12=28} > P_{A4=20}$ (Wüthrich, 1986), constrained by $P_{A12=28} - P_{A4=20} > 10°$ (Table 1). For $A_{4=20}$, we select H8($G_{6/22}$) (the slash indicating overlapped cross peaks) and H6($T_{5=21}$) planes in the acquisition dimension, i.e. magnetization transfers (2). Table 3 further indicates that I_{3D}[H4'($A_{4=20}$)-H1'($A_{4=20}$)-H6($T_{5=21}$)] is less than I_{3D}[H4'($T_{5=21}$)-H1'($T_{5=21}$)-H8($G_{6/22}$)]. As at 300 ms I_{2D}[H1'($A_{4=20}$)-H8($T_{5=21}$)] is found to be greater than I_{2D}[H1'($T_{5=21}$)-H8($G_{6/22}$)] (Table 3), it is deduced that I_{2D}[H4'($A_{4=20}$)-H1'($A_{4=20}$)] is less than I_{2D}[H4'($T_{5=21}$)-H1'($T_{5=21}$)]. Thus, $P_{A4=20} > P_{T5=21}$, and is constrained by $P_{A4=20} - P_{T5=21} > 10°$ (Table 1). As mentioned above, the H1'-H4' intranucleotide cross peak of A_7 is overlapped with that of $A_{4=20}$. We select the H6(C_8) and H8(G_{25}) acquisition planes, as they are well separated. The [H4'(A_{23})-H1'(A_{23})-H8(G_{25})] and [H4'(A_7)-H1'(A_7)-H6(C_8)] magnetization transfers, as well as Table 3, further show that P_{A23} and P_{A7} are essentially the same, which is represented in Table 3 by $5° > P_{A23} - P_{A7} > -5°$.

The intensities of H1'-H4' intranucleotide 2D cross peaks of C_{11} and C_{27} are not measurable, as these are overlapped with other cross peaks (Table 2). Selection of the H8($A_{12=28}$) (ω3) plane in 3D experiments permits us to have access to [H4'(C_{11})-H1'(C_{11})-H8(A_{12})] and [H4'(C_{27})-H1'(C_{27})-H8(A_{28})] 3D cross peaks, even if these two cross peaks remain superimposed in 3D spectra (magnetization transfer (2)). The data from Table 3 yield:

$$I_{3D}[H4'(C_{11/27})\text{-}H1'(C_{11/27})\text{-}H8(A_{12=28})] \approx I_{3D}[H4'(T_{5=21})\text{-}H1'(T_{5=21})\text{-}H8(G_{6/22})] \quad (2)$$

and also indicate that I_{2D}[H1'(C_{11})-H8(A_{12})] and

I_{2D}[H1'(C_{27})-H8(A_{28})] are similar, with their sum similar to I_{2D}[H1'($T_{5=21}$)-H8($G_{6/22}$)]. From this and Eq. 2 we can deduce through the preceding reasonings that I_{2D}[H4'($C_{11/27}$)-H1'($C_{11/27}$)] and I_{2D}[H4'($T_{5=21}$)-H1'($T_{5=21}$)] are similar. Actually, the strong intensity provided by overlapped peaks [H4'($C_{11/27}$)-H1'($C_{11/27}$)] is comparable to that generally noted for pyrimidine residues (Table 1).

The H1'-H4' intranucleotide 2D cross peak of G_6 overlaps with that of G_{22} (Table 2). The H8(A_7) and H8(A_{23}) acquisition planes are well separated and allow selection of the [H4'(G_6)-H1'(G_6)-H8(A_7)] and [H4'(G_{22})-H1'(G_{22})-H8(A_{23})] magnetization transfers. Table 3 indicates that P_{G6} should be greater than P_{G22} (i.e. $P_{G6} - P_{G22} > 10°$ (Table 1)). Here, the phase of G_6 is found to be similar to those of A_{23} and $A_{12=28}$, and the phase of G_{22} is similar to those of G_3 and A_2.

The last example concerns residues A_{23} and T_{10}. The [H4'(T_{10})-H1'(T_{10})-H6(T_{10})] and [H4'(A_{23})-H1'(A_{23})-H8(A_{23})] magnetization transfers and Table 3 confirm that P_{T10} is smaller than P_{A23} (Table 1).

In conclusion, we propose a new method combining 2D and 3D experiments for determining sugar ring conformations. This method can be valuable for rather large oligonucleotides, where signal overlap is a common feature.

Acknowledgements

This work was supported by the Ligue Nationale contre le Cancer and the Association pour la Recherche contre le Cancer. M.C. is a fellow of the Institut de Formation Supérieure Biomédicale. The authors thank Ryan Turner for having proof read the paper.

References

Baleja, J.D., Germann, M.W., Van de Sande, J.-H. and Sykes, B.D. (1990a) *J. Mol. Biol.*, **215**, 411–428.

Baleja, J.D., Moult, J. and Sykes, B.D. (1990b) *J. Magn. Reson.*, **87**, 375–384.

Bernstein, R., Ross, A., Cieslar, C. and Holak, T.A. (1993) *J. Magn. Reson.*, **B101**, 185–188.

Boelens, R., Vuister, G.W., Koning, T.M.G. and Kaptein, R. (1989) *J. Am. Chem. Soc.*, **111**, 8525–8526.

Bonvin, A.M.J.J., Boelens, R. and Kaptein, R. (1991) *J. Magn. Reson.*, **95**, 626–631.

Chuprina, V.P., Nerdal, W., Sletten, E., Poltev, V.I. and Federoff, O.Y. (1993) *J. Biomol. Struct. Dyn.*, **11**, 671–683.

Dietrich, W., Rudel, C.H. and Neumann, M. (1991) *J. Magn. Reson.*, **91**, 1–11.

Donne, D.G., Gozansky, E.K. and Gorenstein, D.G. (1995) *J. Magn. Reson.*, **B106**, 156–163.

Gochin, M. and James, T.L. (1990) *Biochemistry*, **29**, 11172–11180.

Gochin, M., Zon, G. and James, T.L. (1990) *Biochemistry*, **29**, 11161–11171.

Griesinger, C., Sørensen, O.W. and Ernst, R.R. (1989) *J. Mol. Biol.*, **228**, 156–169.

Habazettl, J., Schleicher, M., Otlewski, J. and Holak, T.A. (1992) *J. Magn. Reson.*, **97**, 511–521.

Holak, T.A., Habazettl, J., Oschkinat, H. and Otlewski, J. (1991) *J. Am. Chem. Soc.*, **113**, 3196–3198.

Hosur, R.V., Ravikumar, M., Chary, K.V.R., Sheth, A., Govil, G., Zu-Kun, T. and Miles, H.T. (1986) *FEBS Lett.*, **205**, 71–76.

Karin, M., Liu, Z. and Zandi, E. (1997) *Curr. Opin. Cell Biol.*, **9**, 240–246.

Kim, S.-G., Lin, L.-J. and Reid, B.R. (1992) *Biochemistry*, **31**, 3564–3574.

Lefebvre, A., Mauffret, O., Hartmann, B., Lescot, E. and Fermandjian, S. (1995) *Biochemistry*, **34**, 12019–12028.

Mauffret, O., Hartmann, B., Convert, O., Lavery, R. and Fermandjian, S. (1992) *J. Mol. Biol.*, **227**, 852–875.

Piantini, U., Sørensen, O.W. and Ernst, R.R. (1982) *J. Am. Chem. Soc.*, **104**, 6800–6801.

Poncin, M., Hartmann, B. and Lavery, R. (1992) *J. Mol. Biol.*, **226**, 775–794.

Rance, M., Sørensen, O.W., Bodenhausen, G., Wagner, G., Ernst, R.R. and Wüthrich, K. (1983) *Biochem. Biophys. Res. Commun.*, **117**, 479–485.

Van Wijk, J., Huckriede, B.D., Ippel, J.H. and Altona, C. (1992) *Methods Enzymol.*, **211**, 286–306.

Widmer, H. and Wüthrich, K. (1987) *J. Magn. Reson.*, **74**, 316–336.

Wüthrich, K. (1986) *NMR of Proteins and Nucleic Acids*, Wiley, New York, NY, U.S.A.